Strong glucose dependence of electron current in human monocytes

Boris Musset, Vladimir V. Cherny and Thomas E. DeCoursey

Strong glucose dependence of electron current in human monocytes

Boris Musset, Vladimir V. Cherny, and Thomas E. DeCoursey

Department of Molecular Biophysics and Physiology, Rush University Medical Center, Chicago, Illinois

Musset B, Cherny VV, DeCoursey TE. Strong glucose dependence of electron current in human monocytes. *Am J Physiol Cell Physiol* 302: C286–C295, 2012. First published October 19, 2011; doi:10.1152/ajpcell.00335.2011.—Reactive oxygen species (ROS) production by human monocytes differs profoundly from that by neutrophils and eosinophils in its dependence on external media glucose. Activated granulocytes produce vast amounts of ROS, even in the absence of glucose. Human peripheral blood monocytes (PBM), in contrast, are suspected not to be able to produce any ROS if glucose is absent from the media. Here we compare ROS production by monocytes and neutrophils, measured electrophysiologically on a single-cell level. Perforated-patch-clamp measurements revealed that electron current appeared after stimulation of PBM with phorbol myristate acetate. Electron current reflects the translocation of electrons through the NADPH oxidase, the main source of ROS production. The electron current was nearly abolished by omitting glucose from the media. Furthermore, in preactivated glucose-deprived cells, electron current appeared immediately with the addition of glucose to the bath. To characterize glucose dependence of PBM further, NADPH oxidase activity was assessed as hydrogen peroxide (H_2O_2) production and was recorded fluorometrically. H_2O_2 production exhibited similar glucose dependence as did electron current. We show fundamental differences in the glucose dependence of ROS in human monocytes compared with human neutrophils.

phagocyte; NADPH oxidase; reactive oxygen species; patch-clamp

PERIPHERAL BLOOD MONOCYTES (PBM) are the second most common phagocytes in human blood. As phagocytes, monocytes are able to ingest and destroy bacteria. During the destruction of bacteria, monocytes undergo a respiratory burst. The respiratory burst is an increase in oxygen consumption of the phagocyte, sometimes >50-fold higher than the "normal" oxygen consumption (2). During the oxidative burst, molecular oxygen is reduced into $O_2^{\cdot -}$, which is rapidly converted into H_2O_2. Neither H_2O_2 nor $O_2^{\cdot -}$ is strongly microbicidal, but they are the substrates for all further biological microbicidal compounds, mainly hypochlorite and the hydroxyl radical.

The enzyme responsible for this huge oxygen consumption is the NADPH oxidase complex (5). For granulocytes (neutrophils and eosinophils), it has been shown that the activity of NADPH oxidase can be measured as electron current with the patch-clamp technique (53). Electron current is generated by NADPH oxidase during translocation of electrons from NADPH across the membrane to reduce molecular oxygen on the other side of the membrane. In resting phagocytes, NADPH oxidase is inactive. During activation, its several components assemble at the plasma membrane. After the NADPH oxidase complex has assembled it becomes active, and NADPH is oxidized and electrons translocated; this state corresponds to the active NADPH oxidase. During this process, H^+ are released to the cytosol.

With the translocation of electrons, the transmembrane potential of a phagocyte depolarizes in direction of the quasi reversal potential of electrons. This quasi reversal potential is determined by the redox potential for NADPH and the redox potential for $O_2^{\cdot -}$ and calculated around +160 mV (11). To prevent this massive depolarization, which will stop the respiratory burst, voltage-gated proton channels open to compensate the charge.

PBMs produce superoxide at a rate (47, 58) that can be estimated to be sufficient to generate detectable electron current during perforated-patch-clamp measurements (15). Furthermore, human PBMs exhibit voltage-gated proton current (13, 48). They thus have the same apparatus needed for an oxidative burst as neutrophils and eosinophils: the NADPH oxidase and voltage-gated proton channels, which are essential for charge compensation of the electron translocation (10, 18, 28).

Both NADPH oxidase and voltage-gated proton channels share a number of common regulatory pathways. They are activated by the protein kinase C activator PMA. The PKC inhibitor GF109203X (GFX) prevents activation by PMA. If applied after PMA activation is complete, GFX inhibits the electron current and partially reverses the enhanced proton current (39, 43).

The functional link between proton channels and NADPH oxidase through charge compensation is shown by the inhibition of proton channels (18) in cytochrome *c* reduction measurements. Inhibition of proton current during an oxidative burst leads to a massive depolarization (19, 28, 42), which reduces the amount of superoxide production (27). The reduction of electron current is explained by the voltage dependence of the NADPH oxidase (18). In addition, proton efflux through proton channels counteracts the tendency toward cytosolic acidification, which itself can inhibit NADPH oxidase (40).

Proton current inhibition is achieved by polyvalent metal ions, most potently by Zn^{2+}, which slows activation and shifts the threshold of the proton channel positively (7). The shift in threshold and the slowing of opening diminishes the compensatory function of proton channels and increases the speed and amplitude of depolarization (3, 4, 19, 28, 42), as well as acidification in neutrophils (38). Both depolarization and acidification contribute to inhibiting NADPH oxidase.

In granulocytes the proton current is dramatically changed through stimulation with PMA, entering the "enhanced gating mode." In human eosinophils, the amplitude of the proton conductance increased ~3.9 times, the kinetics of outward currents became faster (activation time constant, τ_{act}) ~3.4 times, and the tail current kinetics got slower (tail current time constant, τ_{tail}) ~3.1 times (44). Additionally, the proton conductance-voltage (g_H-V) relationship shifted negatively with PMA stimulation. The proton channel has a threshold near +20 mV at symmetrical pH. After activation, the threshold shifts by −40 mV. Therefore, in some activated cells, inward proton current can be detected at voltages below the reversal potential for protons. Here we inves-

tigate the properties of the enhanced gating mode of proton channels in human PBMs.

In neutrophils and eosinophils, DPI, an inhibitor of NADPH oxidase, reduces the electron current but also reverses the prolonged tail current kinetics of "activated" proton currents. However, DPI does not change the outward current kinetics, the threshold, or maximal amplitude of the proton current. DPI effects on the proton current have not yet been studied in human PBMs, neither has electron current been recorded.

Finally, we investigate the dogma of strong glucose dependence of the oxidative burst in human PBMs. Strong glucose dependence has been shown for cell lines representing human PBMs (32), but human cells have so far not been investigated. Granulocyte electron current is measurable without glucose added in bath (14, 15). For PBMs, the glucose dependence has not been characterized with the patch-clamp technique.

MATERIALS AND METHODS

PBM isolation. Venous blood samples were drawn from healthy adult volunteers under informed consent according to procedures approved by Rush University Institutional Review Board and in accordance with federal regulations. PBMs were isolated with density gradient centrifugation as described previously (26) with one modification. After plating the peripheral blood mononuclear cells, no growth factors or maturation stimuli were added. After 2 h adherence time, the cells were washed twice with RPMI to remove nonadherent cells. PBM purity was estimated between 80 and 90%. The cells were kept in RPMI with FBS in the incubator until measurement. Every 2 days, the medium was exchanged.

Neutrophil isolation. Neutrophils were isolated as described (15).

Hydrogen peroxide production. Hydrogen peroxide production was measured using Kit 12212 (Molecular Probes, Eugene, OR) essentially as described by the manufacturer, with one exception; the recommended phosphate buffer was replaced by phosphate-free Ringer solution, as described below in *Electrophysiology.* Phosphate was exchanged to prevent it from buffering multivalent cations, including zinc.

Purified PBMs were trypsinized or detached by being put on ice for 10 min and then were counted with a hemocytometer. Equal cell numbers (10,000–40,000) were pipetted into a 96-well plate (Costar, Acton, MA). Zinc ranging from 30 μM to 3 mM was added to test inhibition of H_2O_2 production. Directly before the start of the experiment, 60 nM PMA was added. The measurement was done in a Viktor[3] V 1420 multilabel counter (Perkin Elmer, Waltham, MA) with an absorbance at 563 nm, recording at 2-min intervals. The total incubation volume was 100 μl and the recording lasted 48–180 min.

Electrophysiology. PBMs were studied after 1, 2, or 3 days in culture. PBMs were plated on glass chips which were transferred to the recording chamber. For measurements, PBMs were chosen by morphological criteria. The main criterion was adherence, but also elongated cells were preferred.

For perforated-patch recording, the pipette and bath solutions usually contained 50 mM NH_4^+ in the form of 25 mM $(NH_4)_2SO_4$, 2 mM $MgCl_2$, 1.5 mM $CaCl_2$, 10 mM Bes, 1 mM EGTA, 130 mM $TMAMeSO_3$, and was adjusted to pH 7.0 with TMAOH.

We added 0.5 mg/ml solubilized amphotericin B (~45% purity) (Sigma Chemical, St. Louis, MO) to the pipette solution, after first dipping the tip in amphotericin-free solution.

Micropipettes were pulled using a Flaming-Brown automatic pipette puller (Sutter Instruments, San Rafael, CA) from 7052 glass (Garner Glass, Claremont, CA), coated with Sylgard 184 (Dow Corning, Midland, MI), and heat polished to a tip resistance ranging typically between 3 and 10 MΩ. Electrical contact with the pipette solution was achieved by a thin chlorided silver wire. A reference electrode made from an Ag-AgCl pellet was connected to the bath

through an agar bridge made with Ringer solution [containing (in mM) 160 NaCl, 4.5 KCl, 2 $CaCl_2$, 1 $MgCl_2$, 5 HEPES, adjusted to pH 7.4]. An Axopatch 200B amplifier from Axon (Axon Instruments, Foster City, CA) was used to perform voltage-clamp measurements. All data were acquired with a sampling rate of 500 Hz and low pass filtering at 20 Hz.

Seals were formed with Ringer solution in the bath, and the potential was zeroed after the pipette was in contact with the cell. The bath temperature was usually kept at 20–21°C by a temperature controller (Brook Industries, Lake Villa, IL) and monitored by a resistance temperature detector device. For the higher-temperature measurements, the temperature was adjusted to 25°C.

The average capacity of PBMs was 7.3 ± 1.9 pF ($n = 18$) the first day, 10.8 ± 3.7 pF ($n = 32$) the second day, and 12 ± 4.5 pF ($n = 10$) the third day in culture.

Bath solution changes. Solutions and physiologically active substances were applied by flushing the entire bath solution (~300 μl volume) with ~10 bath volumes, which took ~10–20 s. The time of a bath change was taken roughly as the time of the first volume replacement occurred. The chamber was not perfused continuously. As a control for mechanically induced responses, the bath solution was usually first replaced with an identical solution, transiently increasing H^+ currents due to a small increase in temperature. Because of the strong temperature sensitivity of the H^+ current (12, 34), even a 1°C change has a definite effect. In some experiments (where mentioned), the substances were pipetted directly to the bath, and stirred.

Conventions. Currents and voltages are presented in the normal sense: upward currents represent positive charge flowing outward through the membrane, and potentials are expressed relative to the potential of the original bath solution which is defined as 0 mV. Currents records are presented without correction of leak current or liquid junction potentials.

Determination of conductance. One of the most common problems with the measurement of proton currents is the depletion of protons during a depolarizing pulse. Depletion occurs especially if the pulses are long, as they are in this work. Longer pulses facilitate accurate determination of threshold and resolving small inward or outward currents. We could not avoid depletion in this work, so to obtain the most reasonable values of the proton conductance, g_H, we calculated the conductance $(I_{end} - I_{tail})/(V_{test} - V_{hold})$, where I_{end} is current at the end of each pulse, I_{tail} is tail current amplitude, V_{test} is test potential, and V_{hold} is holding potential, as previously described (45).

In a second method, the conductance was calculated from the maximal current of a pulse and the reversal potential derived from tail currents.

In a third method, outward currents were fitted with a single exponential equation and extrapolated to estimate the maximal amplitude. The method used is given in figure legends.

Analysis of the electron current. Because the electron current equivalent calculated from $O_2^{\cdot-}$ measurements in monocytes (60) is several times smaller than in eosinophils and distinctly smaller than in neutrophils, it is difficult to accurately determine its amplitude in single cells. In this work the following protocol was used. The change of the current at the holding potential after PMA or DPI application is considered to reflect the appearance or inhibition, respectively, of electron current. The holding potential was either −30 mV, −40 mV, or −50 mV. Electron current is nearly voltage independent in this voltage range (18). In most of the cases, the PMA-initiated inward electron current was partially, but not completely reversed by DPI. The impression was received that if PMA remained in the bath solution when DPI was applied, less inhibition of the electron current was observed than when PMA was replaced by DPI with a complete bath exchange. Both bath exchange and direct DPI application were used to analyze the electron current.

A further method for analyzing the electron current was to determine the "leak" before and after application of 60 nM PMA. The leak

current reversal potential was first determined by linear interpolation at $+40$ mV (at the start of the pulse) and -40 mV holding potential. The amplitude of current at the leak reversal potential after PMA stimulation was defined as electron current. The approach makes it possible to estimate electron current during changing leak currents. This method results in 5–10% smaller values as defined by the change of holding potential current in glucose-containing solutions, which in part may reflect the weak voltage dependence of the electron current (I_e) negative to 0 mV (15). Values given for I_e in Fig. 1 were calculated by this method. Current recordings were median filtered (to show electron current without proton currents).

Data analysis. All data were analyzed and graphs were fitted with Origin Software (Origin Lab, Northampton, MA). Single exponential fits were used to determine activation time constant (τ_{act}) and tail current time constant (τ_{tail}). The delay in activation of the outward current was not included in the fitting procedure.

RESULTS

Electron current in human PBMs. To directly measure electron current in human PBMs, we used perforated patch with NH_4^+ as a small mobile buffer, which provided robust control of the pH (described in detail later) inside and outside the cell. Figure 1, *A–C*, displays electron current stimulated by PMA at 20°C at pH 7. As expected from previous literature data (Table 2), electron current in PBMs is much smaller than in human polymorphonuclear leukocytes (PMNs). There were considerable difficulties resolving the electron current without glucose as can be seen in Fig. 1*A*. DPI had an inconclusive influence on the electron current in this cell, but did decrease τ_{tail} of proton currents, which (as will be shown in Fig. 2, *B* and

Fig. 1. Electron currents in human monocytes with and without glucose in the bath solution. Increased electron current at higher temperature and effects of glucose. *A*: electron current recorded in a peripheral blood monocyte (PBM) activated by 60 nM PMA without glucose in the bath solution. *B*: electron current elicited in a solution containing 5 mM glucose. Electron current was slowly reduced by 20 μM DPI. *C*: in this preactivated PBM, addition of glucose increased the electron current immediately. Subsequent addition of PMA did not increase the electron current, but 3 μM GF109203X (GFX) reduced the electron current. *D*: mean electron current in PBMs cultured for 1–3 days in the absence or presence of 5 mM glucose (GLC) at room temperature and with 5 mM glucose at 25°C. Data are displayed as means ± SE. Numbers of cells are given in each bar. No statistical differences could be detected at different times in culture. *E*: data from *D* with measurements at all times in culture pooled for cells studied without glucose, with 5 mM glucose, and with 5 mM glucose at 25°C. ***$P < 0.01$, significant differences between the third and the first two columns. Glucose vs. no glucose electron currents had a significant difference with $P < 0.05$. *F*: a spontaneously activated cell shows a sudden, drastic increase of electron current immediately upon addition of 5 mM glucose. PMA (60 nM) did not increase the electron current further. DPI (20 μM) decreased the electron current. *G*: electron current at 25°C in a PBM supplied with glucose and activated by PMA. The withdrawal of glucose reduced the electron current. Reapplication of glucose restored the electron current. The electron current was inhibited by 20 μM DPI.
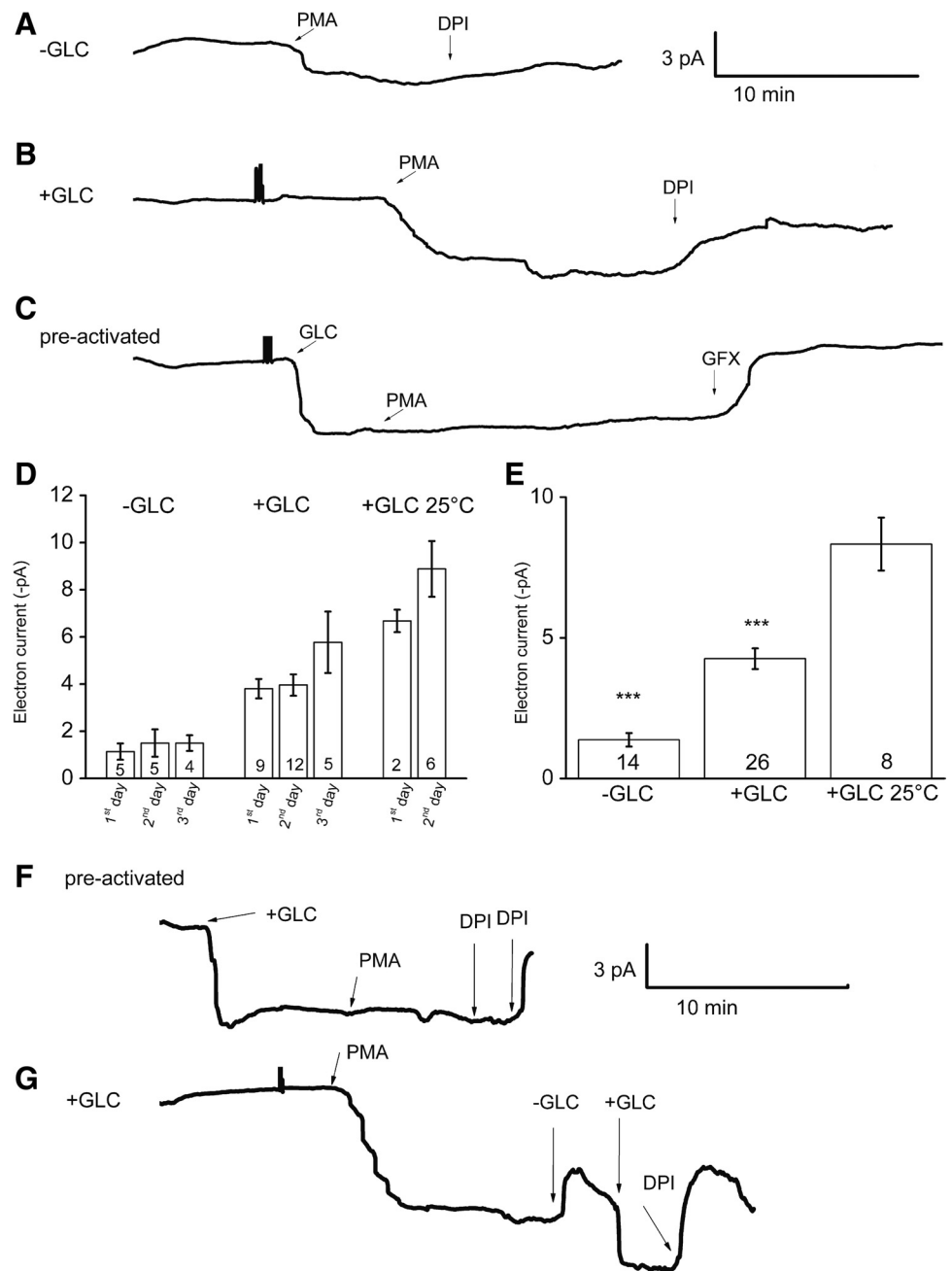
C) is an indicator of prior activation of electron current. Electron currents were more readily detected when glucose was present in the bath. Figure 1*B* shows an electron current measurement in another human PBM. Here 5 mM glucose was added before the measurement. A distinct inward electron current during PMA stimulation is evident. DPI inhibited the electron current, although not completely.

Spontaneously active PBMs can be identified in perforated-patch studies by a more negative threshold of proton currents before stimulation. Figure 1*C* illustrates such a cell in which the proton conductance had a threshold of 0 mV. When 5 mM glucose was added to the bath solution without glucose, electron current appeared immediately. We tested the extent of activation, by addition of 60 nM PMA, which did not activate further electron current, suggesting that the cell was already fully activated. After application of the PKC inhibitor GFX, most of the putative electron current was inhibited. These measurements demonstrate convincingly that glucose has a rapid effect on electron current in human PBMs.

Even under conditions of 20°C and 5 mM glucose, the electron current in human PBMs was small and changes were difficult to measure. To further evaluate whether the removal of glucose has a distinct effect on electron current, the recording temperature was elevated by 5°C. At 25°C, the electron current should be almost twice as big in a perforated-patch measurement, because the Q_{10} (the factor by which the current increases when the temperature increases by 10°C) is ~4 as measured by Morgan et al. (41).

To verify our findings with preactivated PBMs, we repeated the electron current measurements at 25°C. In our hands the electron current on average was around twice bigger than at 20°C. In Fig. 1*F*, a spontaneously active PBM exhibits the same rapid increase in electron current during application of glucose as seen in Fig. 1*C*. Most of the electron current was inhibited by DPI.

Figure 1*G* shows a typical recording from a PBM at 25°C and bathed in 5 mM glucose. After full activation of electron current by PMA, the glucose solution was replaced by glucose-free bath solution. An immediate drop in electron current followed. After changing the bath solution back to 5 mM glucose, electron current reappeared rapidly in nearly the same amount. The electron current was inhibited by DPI. The baseline drift in this experiment was probably due to a gradual increase in leak current.

We summarized our findings in Fig. 1, *D* and *E*, to illustrate the effects of glucose and temperature on electron current in human PBMs. Figure 1*D* shows that there are negligible differences in PBM electron currents depending on the length of time in culture. Measured in the absence of glucose, the PBM electron current is the smallest of all other human phagocytes.

Proton current in human PBMs shows no glucose dependence. PBMs were studied using the perforated-patch approach to preserve intracellular second messenger pathways. To study proton currents, pH control is essential because proton currents are sensitive to pH, which directly influences their voltage dependence and kinetics. Symmetrical pH was established to isolate effects of activators and inhibitors from spurious effects of pH changes. NH_4^+ (50 mM NH_4^+ in bath and pipette solutions) was used to clamp the cell at pH ~7.0, both inside, intracellular pH (pH$_i$), and outside the cell, extracellular pH (pH$_o$). Under these conditions, most human PBMs exhibited robust voltage-gated proton currents, as illustrated in Fig. 2*A*. Reversal potential was

measured with the tail current approach in different pH gradients, established by varying the NH_4^+ concentration. The reversal potential was near the Nernst potential for protons (not shown), confirming proton selectivity.

First we investigated the basic characteristics of the proton channel in human PBMs. Figure 2*A* shows proton currents in a control PBM in a resting, unstimulated state. The outward proton current starts at a threshold of +10 mV, which is recognizable only at higher gain by the appearance of a tail current upon repolarization. At the scale used in Fig. 2, outward current during the +20 mV pulse is distinguishable.

PMA was used to activate human PBMs. Figure 2*B* represents the same PBM measured in Fig. 2*A* after activation with 60 nM PMA. The proton currents show a distinct increase in amplitude, combined with faster activation (a decrease in τ_{act}, Fig. 2*E*). Interestingly and comparable to other phagocytes, the tail currents exhibit a stark slowing in kinetics which is directly evident in the prolonged tail current decay. The conductance is higher than control, and the shift in threshold is evident in the conductance-voltage curve in Fig. 2*D*.

Table 1 summarizes the differences between the properties of control and activated voltage-gated proton currents. In PMA-stimulated PBMs, the outward current activates more rapidly, the tail current deactivates more slowly, and the conductance is higher. After stimulation by PMA, the proton current threshold (the voltage at which distinct proton current is first observed) shifts negatively, on average by −28.3 mV.

DPI inhibits electron current but also influences proton current. Figure 2*C* shows the proton current after inhibition of NADPH oxidase by 20 μM DPI. The proton current has increased slightly in amplitude even after DPI, although the threshold is unchanged, as can been seen in the conductance-voltage curves in Fig. 2*D*. The only apparent change in the currents in Fig. 2*C* is the faster tail current kinetics. In contrast to the tail current, the kinetics of the outward current are unchanged compared with the PMA-activated current (Fig. 2*E*). Thus DPI as an electron current inhibitor influences only one observed proton current parameter, the tail current kinetics. One can divide the proton current parameters into electron current-dependent parameters, namely, the tail current kinetics, and electron current-independent parameters, which are activation kinetics, amplitude, and threshold.

The effect of DPI did not influence the tail current kinetics of nonstimulated cells (data not shown). This has been also reported for neutrophils (15) and eosinophils (14).

In contrast to electron currents, proton currents in human PBMs seemed to be unaffected by the glucose concentration outside the cell. In typical experiments, test pulses were applied every 38 s during addition or removal of glucose from the bath, and no consistent immediate changes in the proton current were observed (not shown). Table 1 shows that the changes of the proton current parameters after stimulation with PMA were similar with or without glucose and with glucose at 25°C.

H_2O_2 release by PBM: glucose dependence. The glucose dependence of electron current suggests that the oxygen radical production (H_2O_2 production) should also exhibit glucose dependence. Figure 3*A* shows a clear difference in the rate of H_2O_2 production in PBMs studied with or without 5 mM glucose in Ringer solution. Eight measurements were pooled
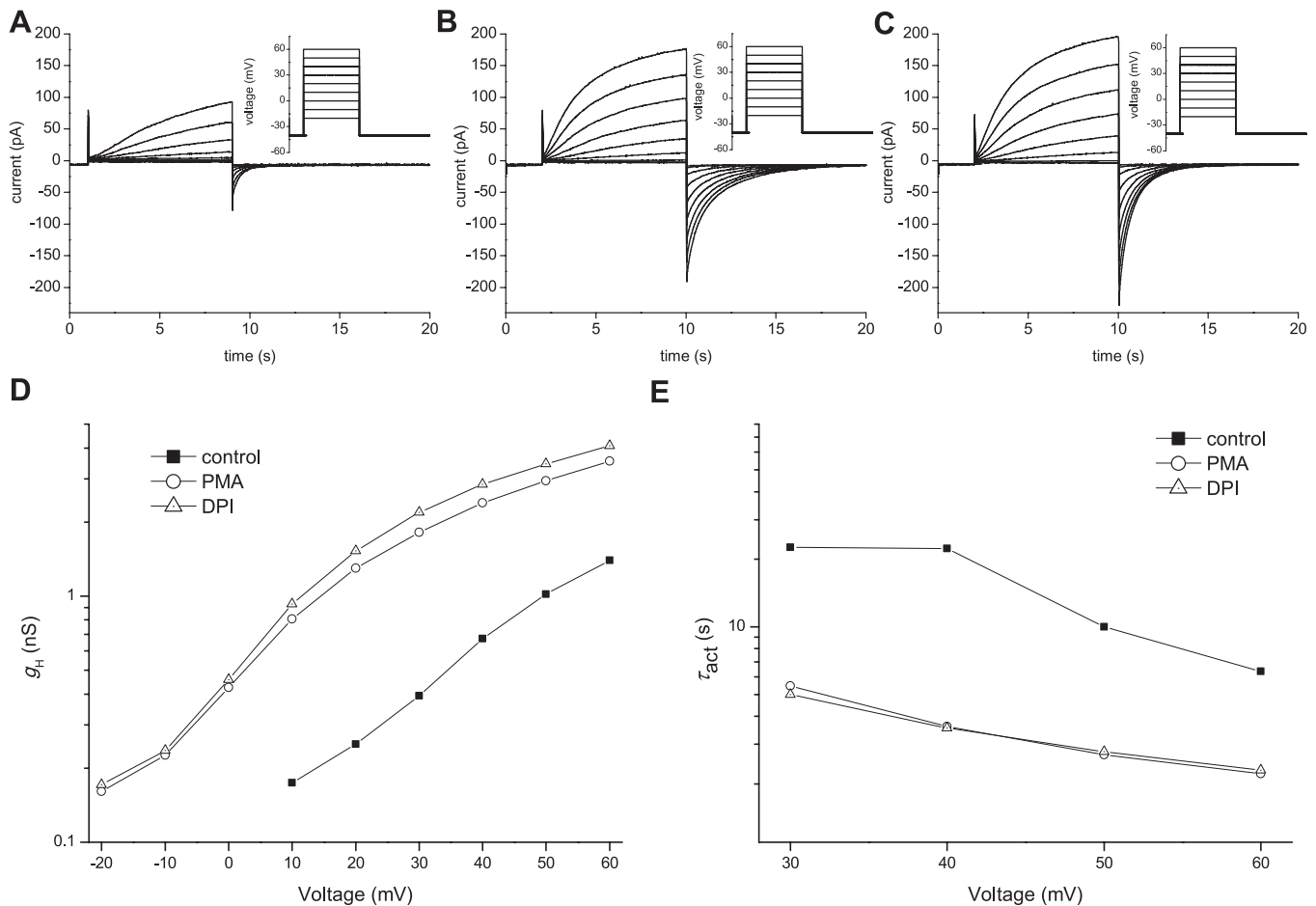
Fig. 2. Comparison of the properties of H$^+$ currents before and after PMA and DPI in a single human monocyte. *A*: currents recorded in a control PBM during depolarizing pulses from holding potential (V_h) = −40 mV to −20 mV through +60 mV in 10-mV increments are superimposed. *B*: currents in the same cell after addition of 60 nM PMA. *C*: currents in the same cell directly after addition of 20 μM DPI and washout of PMA. Currents in *A*, *B*, and *C* are shown at the same current- and time base and were measured with the same protocol. *D*: chord conductance (g_H)-voltage relationship of the proton currents in this cell recorded (control) and in the presence of PMA or DPI. Conductance was calculated from the tail currents (see MATERIALS AND METHODS). *E*: voltage dependence of activation time constant (τ_act) in this monocyte before stimulation (■), after PMA activation (○), and after DPI application (△). In control records during small depolarizations, τ_act was often longer than the pulse; hence in these cases, τ_act was not well determined.

and normalized to show average H$_2$O$_2$ production per cell. It is evident that glucose profoundly enhances H$_2$O$_2$ production.

We further wanted to test whether the H$_2$O$_2$ production in PMNs (neutrophils) has comparable glucose dependence. Identical measurements on human neutrophils are shown in Fig. 3*B*. Neutrophils also exhibit a distinct dependence on glucose in the outer media. However, compared with PBMs, the dependence of neutrophils on glucose is weaker. In Fig. 3*C*, the H$_2$O$_2$ production of an average PBM after 50 min is scaled to the

production of an average neutrophil, emphasizing the different kinetics. After an initial delay, PBMs produce H$_2$O$_2$ tonically at a constant rate, whereas the rate in neutrophils peaks at 10–15 min and declines thereafter. In longer measurements, production of H$_2$O$_2$ by neutrophils virtually ceased after 60 min. Intriguingly, H$_2$O$_2$ production by neutrophils declined whether glucose was present or not. When the data for neutrophils with and without glucose were scaled to the same final point, the time courses superimposed (Fig. 3*C*).

Table 1. *Proton current activation by PMA*

	τ_act (control/PMA)	τ_tail (PMA/control)	g_H (PMA/control)	Threshold, mV (control−PMA)
Monocytes − GLC	4.4 ± 2.7 (6)	4.0 ± 1.4 (6)	3.6 ± 0.8 (6)	28.3 ± 4.1 (6)
Monocytes + GLC	2.3 ± 0.6 (11)	3.5 ± 1.3 (11)	2.7 ± 1.3 (12)	32.5 ± 7.5 (12)
Monocytes + 25°C + GLC	2.9 ± 1.3 (7)	6.51 ± 1.7 (7)	2.7 ± 0.9 (7)	35.7 ± 5.3 (7)

Values are means ± SD (*n*). The four basic biophysical characteristics of the enhanced gating mode of voltage-gated proton channels are given with and without glucose (GLC) and at ~20°C or at 25°C. All outward current kinetics (activation time constant, τ_act) data were measured at +40 mV. All tail current kinetics (tail current constant, τ_tail) data were recorded at −40 mV. Conductance (*g*) was determined by exponential fit to the most depolarizing voltage pulse. Threshold is the voltage at which the proton conductance (g_H) was first detectably activated during families of incrementing voltage pulses. The increased shift of threshold voltage due to the application of glucose was significant at *P* = 0.05 (Student's *t*-test). Control monocyte data in the absence and presence of glucose are from Musset et al. (44).
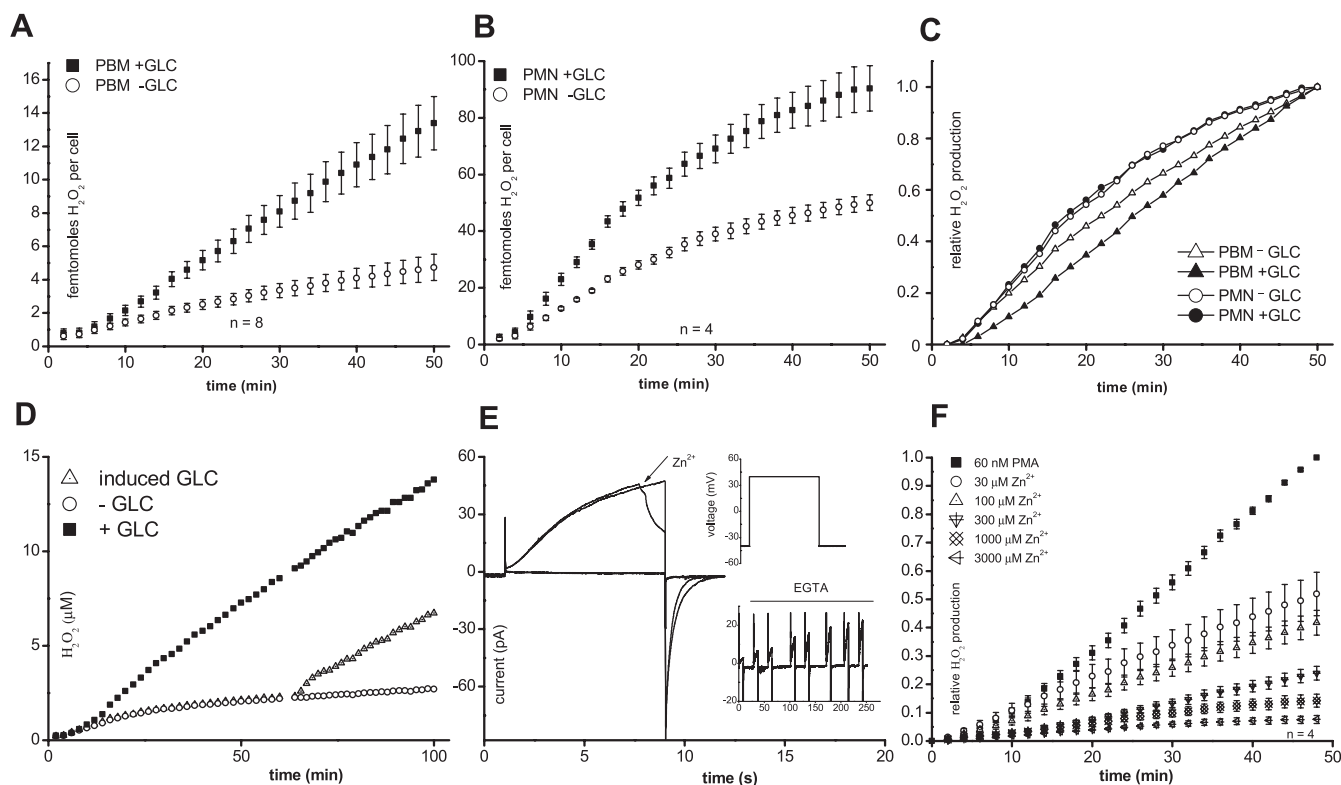
Fig. 3. H_2O_2 release measured with and without glucose (GLC) in human PBMs and neutrophils. Inhibition of proton currents and H_2O_2 release in human monocytes by Zn^{2+}. *A*: H_2O_2 production measured in human monocytes (PBM) in the presence (■) or absence (○) of 5 mM glucose. *B*: glucose dependence of H_2O_2 production in human neutrophils (PMN). *C*: normalization of H_2O_2 production in neutrophils and monocytes from *A* and *B* to the same maximal rate. *D*: H_2O_2 production measured in PBMs with and without glucose. Glucose was added after 60 min to cells without glucose. *E*: proton current in a human PBM during pulses to +40 mV (*inset*). Zn^{2+} (5 μM) inhibited proton current immediately upon addition to the bath. *Inset*: proton current was restored by removal of Zn^{2+} with EGTA. *F*: H_2O_2 production in the absence or presence of Zn^{2+} at the indicated concentrations ranging from 30 μM to 3,000 μM.

In contrast, in PBMs the time courses with and without glucose are distinct.

PBM electron current recorded with the patch-clamp technique was rapidly and reversibly enhanced by addition of glucose. In Fig. 3*D*, we investigated whether this dependence can also be detected in fluorescence measurements of H_2O_2 production by adding glucose during an experiment. PBMs with and without glucose were stimulated by PMA, and after 62 min, glucose was added to the PBMs without glucose. Figure 3*D* shows that the added glucose initiated production of H_2O_2 at the same rate as in PBMs bathed with glucose throughout the experiment. Analogous to the electron current measurements, the initial delay before activation of H_2O_2 production by PMA was absent when glucose was added to cells already activated by PMA in the absence of glucose. Evidently, the NADPH oxidase complexes in both experiments were assembled and active, but simply were operating at a lower rate without glucose.

Zinc dependence of reactive oxygen species production in PBMs. To answer the question whether in PBMs proton channels also support NADPH oxidase activity as in phagocytes, we investigated Zn^{2+} inhibition of proton channels in PBMs. In Fig. 3*E*, the rapid block of proton currents by Zn^{2+} in patch-clamp measurements in PBMs is shown. The *inset* shows that the inhibition by 5 μM Zn^{2+} was reversible upon EGTA application. Furthermore, we were interested in whether inhibiting proton channels would have a comparable effect on H_2O_2 production in human PBMs as in neutrophils.

Figure 3*F* displays the inhibition of H_2O_2 production by different concentrations of Zn^{2+}. After ~50 min, H_2O_2 production was reduced ~50% by 30 μM Zn^{2+}. The inhibition of H_2O_2 production by Zn^{2+} in PBMs is comparable to that in PMN (21).

DISCUSSION

Electrophysiology of the monocyte respiratory burst. One of the aims of this study was to investigate the properties of electron currents and proton currents and their relationship in resting and activated human PBMs. We compared them with those in other phagocytes, with a special focus on metabolic differences. Although monocytes were reported to express proton channels (13, 48) and produce $O_2^{·−}$ via NADPH oxidase (Table 2), the coordinated activation of these molecules during the respiratory burst had not been studied. Because monocytes (31) and macrophages (23, 37) express a much larger variety of ion channels than neutrophils or eosinophils (21, 22), it was possible that other ion channels in PBMs might carry out some of the functions of proton channels in granulocytes. In particular, eosinophils lack outward K^+ currents (21), whereas PBMs and related cells express both voltage-activated ($K_V1.3$) and Ca^{2+}-activated (BK) K^+ channels (16, 20, 24, 51).

With respect to their voltage dependence, activation and deactivation kinetics, and sensitivity to Zn^{2+}, proton currents in unstimulated PBMs were similar to proton currents in all other phagocytes. The characteristics of enhanced gating of

Table 2. *Electron current equivalent per human monocyte*

Stimulus	Electron Current, pA	Method	Glucose, mM	Reference
PMA	1.07–4.92	H_2O_2	10	(47)
Opsonized zymosan	2.56	H_2O_2	5	(49)
PMA	0.89–2.61	H_2O_2	10	(58)
PMA	1.71	$O_2{}^{\cdot-}$	5	(57)
PMA	0.80–2.00	$O_2{}^{\cdot-}$	5	(26)
PMA	2.42	H_2O_2	5	(6)
PMA	2.98	$O_2{}^{\cdot-}$	Not known	(60)
PMA	1.03	H_2O_2	5	This study-PBM
PMA	10.81	H_2O_2	5	This study-PMN

Electron current was calculated from different studies of human monocytes. Electron current equivalent was calculated from superoxide, cytochrome *c* reduction, or H_2O_2 measurements on human monocytes in previous studies. Amplex Red results in peripheral blood monocytes (PBM) and polymorphonuclear leukocytes (PMN) (neutrophils) in the present study are also given.

proton channels produced by PMA stimulation of human PBMs were similar in PBMs cultured 1, 2, or 3 days. In most respects the PMA response was identical to that in other phagocytes. One subtle difference in the PMA response was that, during activation, the shift in threshold voltage ($V_{threshold}$) for PBMs was somewhat smaller than that for neutrophils or eosinophils and was closer to −30 mV than −40 mV (14). There appeared to be a correlation between the size of the electron current and the shift in threshold in PBMs. The shift of $V_{threshold}$ (Table 1) and the I_e amplitude (Fig. 1E) in PBMs both increased when glucose was included in the bath, and both increased further when the temperature was increased. Consistent with this observation, the shift of $V_{threshold}$ in human basophils, which lack NADPH oxidase and hence I_e, was only −20 mV (46). The mechanism by which the electron current might influence the $V_{threshold}$ shift is at present highly speculative. One suggestion is that NADPH oxidase locally decreases pH, which then stabilizes the open state of the proton channel (11, 15).

Metabolic differences. In this study the physiological concentration of 5 mM glucose was used to investigate the dependence of proton current and electron current on this important energy source of cells. Using glucose leads intuitively to the question of whether there are metabolically controlled ion channels. Some ATP-sensitive K^+ (K_{ATP}) ion channels are dependent indirectly on glucose via β subunits responsive to the ATP/ADP concentration ratio (56). Thus it was conceivable that proton currents might respond to glucose. However, there was no direct dependence of the amplitude or other biophysical properties of proton current on glucose (0 mM or 5 mM glucose), even in the activated state. Since the enhanced gating mode is dependent on phosphorylation (39, 43), it might be reasonable to postulate that if there were no triphosphates in the cell to phosphorylate the channel via PKC, no enhanced gating mode in PBMs should be possible. Experimental data in this study show that there are still enough triphosphates in the cytosol of PBMs even if there is no access to external glucose for up to tens of minutes.

The electron current in PBMs is much smaller than in other phagocytes. Studied in the absence of glucose at 20°C, I_e was only −1.4 pA in monocytes (Fig. 1E), compared with −2.3 pA in human neutrophils (15), and −6.0 pA in human eosinophils (14). It was difficult to measure electron current reliably in PBMs without glucose in the bath solution. Glucose facilitated the measurement of electron current in PBM by increasing the I_e amplitude threefold (Fig. 1E). The dependence on glucose was most apparent when the cells were already activated before glucose was added. In this situation, I_e increased

immediately upon glucose addition (Fig. 1, C and F), in contrast with the gradual increase of I_e over several minutes when PMA is first introduced to resting cells (Fig. 1, B and G). Presumably, the slow PMA response reflects the progressive phosphorylation of NADPH oxidase components, which then migrate to the membrane and assemble to form active complexes. The rapid glucose response reflects the rapid conversion of glucose into NADPH to provide substrate for NADPH oxidase complexes that are already assembled and operational.

Simple considerations of geometry suggest that the glucose response should occur rapidly. If one assumes that there is 50 μM NADPH in a preactivated cell (17) in the monocyte cytoplasm, a typical capacity of the cell of 10 pF in a cylindrical cell of height 1 μm, an electron current of −4.5 pA (Fig. 1E, with glucose), then a complete turnover of the cytoplasmic NADPH would occur in ~1 s.

Also a second approach can be used to approximate glucose response time. We compared turnover rates of the key enzymes from glucose transport to hexose monophosphate shunt. The turnover rate of glucose transport from the outside to the inside of the cell is ~1,133 s^{-1} via Glut1, the ubiquitous glucose transporter [K_m [^{14}C]glucose ~1.6 mM zero trans influx 20°C (36)/K_m 6.9 mM measured using 2-deoxyglucose (54)]. But Glut3 is also present in white blood cells, and through PMA activation, Glut3 will be translocated from internal to external membranes. The turnover rate of Glut3 is ~6,500 s^{-1} (54) and the K_m for 2-deoxyglucose is 1.4 mM (room temperature) (9). Since the glucose is immediately phosphorylated by hexokinase [turnover rate ~200 s^{-1} (1)], the glucose gradient to the inside of the cell is robust and steep. Glucose 6 phosphate is the substrate for the hexose monophosphate shunt. Glucose 6 dehydrogenase is the rate limiting enzyme of the hexose monophosphate shunt and has a turnover rate of 120 s^{-1} (8) per subunit. Finally, the NADPH oxidase turnover rate is estimated to be around 300 s^{-1} (11). Since turnover rates vary with substrate concentrations and recording conditions, these numbers give only an approximation of their physiological speed. If we consider the reaction chain as a linear series of fast processes, it is likely that, from the addition of glucose to the electron current, at most only a few seconds elapse.

PBMs and neutrophils differed in the stronger glucose dependence of NADPH oxidase activity in PBMs. Glucose is, together with glycogen, the major substrate to generate NADPH in the cell (2, 29, 55). For macrophages it has been shown that glycogen stores are absent (30). In contrast, neutrophils have large glycogen stores (59); thus there is conver-

sion of glycogen into NADPH (30). This difference in glucose dependence between PBMs and PMN was observed both in fluorescence measurements of H_2O_2 production and in I_e data collected with the patch-clamp technique. Both I_e and the maximum rate of H_2O_2 production were threefold larger in the presence of glucose in PBMs (Figs. 1*E* and 3*A*); for neutrophils the difference in H_2O_2 production was less than twofold (Fig. 3*B*). This result is consistent with the findings of Lin et al. (35). The strong dependence on glucose was thought to be a characteristic of macrophages (32), but our neutrophil measurements showed glucose dependence as well. In the macrophage-related J774.16 cell line, $O_2^{\cdot -}$ production absolutely required glucose after the first few minutes (32). In contrast, human PBMs produced H_2O_2 for an hour or more with no glucose, although at a strongly reduced and gradually declining rate.

Interestingly, pronounced metabolic differences between PBMs and neutrophils have been described (49). First, during their oxidative burst, PBMs use only 30% of total oxygen consumption for the production of $O_2^{\cdot -}$ in contrast to neutrophils, which use essentially all the oxygen for the production of $O_2^{\cdot -}$ (49). This might indicate that activated PBMs also use oxygen for other tasks than radical production which are more oxygen demanding.

The hexose monophosphate shunt is thought to be the main producer of NADPH, which is the substrate for the NADPH oxidase. This metabolic pathway accounts for most of the oxidative burst in human granulocytes (17, 33, 50, 53) and macrophages (32). Thus the basic mechanism for a respiratory burst in neutrophils and PBMs is the same: the hexose monophosphate shunt, proton channels, and NADPH oxidase. A striking difference between PBMs and neutrophils was the time course of H_2O_2 release. Neutrophils terminate their oxidative burst with exactly the same time course whether they are provided with glucose or not (normalized data in Fig. 3*C*). The insensitivity to glucose of the turn-off kinetics indicates that NADPH oxidase deactivation is not due to a loss of substrate generated from glucose. Several ways of terminating the oxidative burst in neutrophils have been discussed, above all, GTPases and phosphatases (17). The present experimental conditions of activating PKC permanently by PMA speak against phosphatases having an impact on the termination of the oxidative burst. PMA appears to stimulate PKC so strongly that phosphatases cannot overcome PKC phosphorylation activity. This can be deduced from patch-clamp measurements. The enhanced gating mode of the proton channel is due to phosphorylation (39, 43) and after PMA stimulation is not reversed during long measurements. But introducing GFX as a kinase inhibitor substantially reversed the enhanced gating mode, apparently by revealing the activity of phosphatases (39).

In contrast to neutrophils, PBMs produce oxygen radicals at a constant rate after PMA stimulation. As Fig. 3*D* shows, H_2O_2 production is sustained nearly 2 h with negligible change in rate. There must be a difference between the termination of the oxidative burst in PBMs and neutrophils during PMA stimulation.

One could speculate that the process of producing oxygen radicals itself could lead to termination in neutrophils due to the high rate. Maybe radicals that are produced outside the cell diffuse back in neutral form into the cell. PBMs are bigger cells and on a single-cell level are weaker, but steady producers of reactive oxygen species (ROS) compared with neutrophils. The rate of H_2O_2 production by a single PBM is 10 times lower than by a neutrophil (Table 2). To compare the density of NADPH oxidase in these two cell types, electron current can be normalized to membrane area, which is indicated by capacity. Electron current in measurements without glucose is -0.14 pA/pF in PBMs and -1.09 pA/pF (14) in neutrophils, an eightfold difference. In eosinophils the capacity is between 1.8–3 pF (3) or 1.2–3.6 pF (52). Assuming a capacity of 2.4 pF and an electron current of -6 pA, electron current density would be -2.5 pA/pF in an eosinophil. Eosinophils stimulated with PMA terminate the oxidative burst after 25 min (14), neutrophils after 60 min, PBMs >120 min. Self-inflicted damage due to high ROS production rates might be expected to be much greater in a neutrophil or an eosinophil than in a PBM. Contradicting this idea, the time course of termination was independent of glucose in the ROS measurements of neutrophils.

Comparison to previous studies. Electron current has never before been measured directly with the patch-clamp technique in human PBMs. Table 2 shows the calculated electron current equivalent from selected publications, which ranges from -0.89 pA to -4.92 pA (6, 25, 47, 49, 57, 58). This variability might reflect differences in experimental setup and culture of the PBMs. The activity of NADPH oxidase estimated from H_2O_2 release (Table 2) was 10 times greater in human neutrophils than in PBMs. In previous studies, human neutrophils produced three to six times more ROS over 30 min than monocytes (6, 49, 60).

The inhibition of H_2O_2 release by Zn^{2+} was similar to that reported in neutrophils (21). These findings lead to the conclusion that in human PBMs, proton and electron currents are the main players during the oxidative burst. The components needed for this physiological phenomenon are thus the same in every phagocyte: voltage-gated proton channels, the hexose monophosphate shunt, and NADPH oxidase. The PBM has a more acute requirement for glucose. Fluctuations in blood glucose levels that occur in diabetes would be expected to have more profound effects on PBMs than on neutrophils.

DISCLOSURES

No conflicts of interest, financial or otherwise, are declared by the author(s).

AUTHOR CONTRIBUTIONS

B.M., V.V.C., and T.E.D. conception and design of research; B.M. performed experiments; B.M. analyzed data; B.M., V.V.C., and T.E.D. interpreted results of experiments; B.M. prepared figures; B.M. drafted manuscript; B.M., V.V.C., and T.E.D. approved final version of manuscript; V.V.C. and T.E.D. edited and revised manuscript.

REFERENCES

1. **Albe KR, Butler MH, Wright BE.** Cellular concentrations of enzymes and their substrates. *J Theor Biol* 143: 163–195, 1990.
2. **Babior BM.** The respiratory burst of phagocytes. *J Clin Invest* 73: 599–601, 1984.

3. **Bánfi B, Schrenzel J, Nüsse O, Lew DP, Ligeti E, Krause KH, Demaurex N.** A novel H$^+$ conductance in eosinophils: unique characteristics and absence in chronic granulomatous disease. *J Exp Med* 190: 183–194, 1999.

4. **Bankers-Fulbright JL, Gleich GJ, Kephart GM, Kita H, O'Grady SM.** Regulation of eosinophil membrane depolarization during NADPH oxidase activation. *J Cell Sci* 116: 3221–3226, 2003.

5. **Bedard K, Krause KH.** The NOX family of ROS-generating NADPH oxidases: physiology and pathophysiology. *Physiol Rev* 87: 245–313, 2007.

6. **Bianca VD, Dusi S, Bianchini E, Dal Pra I, Rossi F.** β-Amyloid activates the O$_2^-$ forming NADPH oxidase in microglia, monocytes, and neutrophils. A possible inflammatory mechanism of neuronal damage in Alzheimer's disease. *J Biol Chem* 274: 15493–15499, 1999.

7. **Cherny VV, DeCoursey TE.** pH-dependent inhibition of voltage-gated H$^+$ currents in rat alveolar epithelial cells by Zn^{2+} and other divalent cations. *J Gen Physiol* 114: 819–838, 1999.

8. **Cohen P, Rosemeyer MA.** Glucose-6-phosphate dehydrogenase from human erythrocytes. *Methods Enzymol* 41: 208–214, 1975.

9. **Colville CA, Seatter MJ, Jess TJ, Gould GW, Thomas HM.** Kinetic analysis of the liver-type (GLUT2) and brain-type (GLUT3) glucose transporters in *Xenopus* oocytes: substrate specificities and effects of transport inhibitors. *Biochem J* 290: 701–706, 1993.

10. **DeCoursey TE.** Interactions between NADPH oxidase and voltage-gated proton channels: why electron transport depends on proton transport. *FEBS Lett* 555: 57–61, 2003.

11. **DeCoursey TE.** Voltage-gated proton channels and other proton transfer pathways. *Physiol Rev* 83: 475–579, 2003.

12. **DeCoursey TE, Cherny VV.** Temperature dependence of voltage-gated H$^+$ currents in human neutrophils, rat alveolar epithelial cells, and mammalian phagocytes. *J Gen Physiol* 112: 503–522, 1998.

13. **DeCoursey TE, Cherny VV.** Voltage-activated proton currents in human THP-1 monocytes. *J Membr Biol* 152: 131–140, 1996.

14. **DeCoursey TE, Cherny VV, DeCoursey AG, Xu W, Thomas LL.** Interactions between NADPH oxidase-related proton and electron currents in human eosinophils. *J Physiol* 535: 767–781, 2001.

15. **DeCoursey TE, Cherny VV, Zhou W, Thomas LL.** Simultaneous activation of NADPH oxidase-related proton and electron currents in human neutrophils. *Proc Natl Acad Sci USA* 97: 6885–6889, 2000.

16. **DeCoursey TE, Kim SY, Silver MR, Quandt FN.** Ion channel expression in PMA-differentiated human THP-1 macrophages. *J Membr Biol* 152: 141–157, 1996.

17. **DeCoursey TE, Ligeti E.** Regulation and termination of NADPH oxidase activity. *Cell Mol Life Sci* 62: 2173–2193, 2005.

18. **DeCoursey TE, Morgan D, Cherny VV.** The voltage dependence of NADPH oxidase reveals why phagocytes need proton channels. *Nature* 422: 531–534, 2003.

19. **Demaurex N, Petheõ GL.** Electron and proton transport by NADPH oxidases. *Philos Trans R Soc Lond B Biol Sci* 360: 2315–2325, 2005.

20. **Essin K, Gollasch M, Rolle S, Weissgerber P, Sausbier M, Bohn E, Autenrieth IB, Ruth P, Luft FC, Nauseef WM, Kettritz R.** BK channels in innate immune functions of neutrophils and macrophages. *Blood* 113: 1326–1331, 2009.

21. **Femling JK, Cherny VV, Morgan D, Rada B, Davis AP, Czirják G, Enyedi P, England SK, Moreland JG, Ligeti E, Nauseef WM, DeCoursey TE.** The antibacterial activity of human neutrophils and eosinophils requires proton channels but not BK channels. *J Gen Physiol* 127: 659–672, 2006.

22. **Gallin EK.** Ion channels in leukocytes. *Physiol Rev* 71: 775–811, 1991.

23. **Gallin EK.** Voltage clamp studies in macrophages from mouse spleen cultures. *Science* 214: 458–460, 1981.

24. **Gallin EK, McKinney LC.** Patch-clamp studies in human macrophages: single-channel and whole-cell characterization of two K$^+$ conductances. *J Membr Biol* 103: 55–66, 1988.

25. **Gudewicz PW, Frewin MB, Heinel LA, Minnear FL.** Priming of human monocyte superoxide production and arachidonic acid metabolism by adherence to collagen- and basement membrane-coated surfaces. *J Leukoc Biol* 55: 423–429, 1994.

26. **Hanley PJ, Musset B, Renigunta V, Limberg SH, Dalpke AH, Sus R, Heeg KM, Preisig-Muller R, Daut J.** Extracellular ATP induces oscillations of intracellular Ca^{2+} and membrane potential and promotes transcription of IL-6 in macrophages. *Proc Natl Acad Sci USA* 101: 9479–9484, 2004.

27. **Henderson LM, Chappell JB, Jones OT.** Internal pH changes associated with the activity of NADPH oxidase of human neutrophils. Further evidence for the presence of an H$^+$ conducting channel. *Biochem J* 251: 563–567, 1988.

28. **Henderson LM, Chappell JB, Jones OT.** The superoxide-generating NADPH oxidase of human neutrophils is electrogenic and associated with an H$^+$ channel. *Biochem J* 246: 325–329, 1987.

29. **Iyer GYN, Islam MF, Quastel JH.** Biochemical aspects of phagocytosis. *Nature* 192: 535–541, 1961.

30. **Karnovsky ML.** Metabolic basis of phagocytic activity. *Physiol Rev* 42: 143–168, 1962.

31. **Kim SY, Silver MR, DeCoursey TE.** Ion channels in human THP-1 monocytes. *J Membr Biol* 152: 117–130, 1996.

32. **Kiyotaki C, Peisach J, Bloom BR.** Oxygen metabolism in cloned macrophage cell lines: glucose dependence of superoxide production, metabolic and spectral analysis. *J Immunol* 132: 857–866, 1984.

33. **Klebanoff SJ.** Intraleukocytic microbicidal defects. *Annu Rev Med* 22: 39–62, 1971.

34. **Kuno M, Ando H, Morihata H, Sakai H, Mori H, Sawada M, Oiki S.** Temperature dependence of proton permeation through a voltage-gated proton channel. *J Gen Physiol* 134: 191–205, 2009.

35. **Lin X, Candlish JK, Thai AC.** Superoxide production by neutrophils from diabetics and normal subjects in response to glucose and galactose. *Exp Mol Pathol* 58: 229–236, 1993.

36. **Lowe AG, Walmsley AR.** The kinetics of glucose transport in human red blood cells. *Biochim Biophys Acta* 857: 146–154, 1986.

37. **McKinney LC, Gallin EK.** Inwardly rectifying whole-cell and single-channel K currents in the murine macrophage cell line J774.1. *J Membr Biol* 103: 41–53, 1988.

38. **Morgan D, Capasso M, Musset B, Cherny VV, Ríos E, Dyer MJ, DeCoursey TE.** Voltage-gated proton channels maintain pH in human neutrophils during phagocytosis. *Proc Natl Acad Sci USA* 106: 18022–18027, 2009.

39. **Morgan D, Cherny VV, Finnegan A, Bollinger J, Gelb MH, DeCoursey TE.** Sustained activation of proton channels and NADPH oxidase in human eosinophils and murine granulocytes requires PKC but not cPLA2 α activity. *J Physiol* 579: 327–344, 2007.

40. **Morgan D, Cherny VV, Murphy R, Katz BZ, DeCoursey TE.** The pH dependence of NADPH oxidase in human eosinophils. *J Physiol* 569: 419–431, 2005.

41. **Morgan D, Cherny VV, Murphy R, Xu W, Thomas LL, DeCoursey TE.** Temperature dependence of NADPH oxidase in human eosinophils. *J Physiol* 550: 447–458, 2003.

42. **Murphy R, DeCoursey TE.** Charge compensation during the phagocyte respiratory burst. *Biochim Biophys Acta* 1757: 996–1011, 2006.

43. **Musset B, Capasso M, Cherny VV, Morgan D, Bhamrah M, Dyer MJ, DeCoursey TE.** Identification of Thr^{29} as a critical phosphorylation site that activates the human proton channel *Hvcn1* in leukocytes. *J Biol Chem* 285: 5117–5121, 2010.

44. **Musset B, Cherny VV, Morgan D, DeCoursey TE.** The intimate and mysterious relationship between proton channels and NADPH oxidase. *FEBS Lett* 583: 7–12, 2009.

45. **Musset B, Cherny VV, Morgan D, Okamura Y, Ramsey IS, Clapham DE, DeCoursey TE.** Detailed comparison of expressed and native voltage-gated proton channel currents. *J Physiol* 586: 2477–2486, 2008.

46. **Musset B, Morgan D, Cherny VV, MacGlashan DW Jr, Thomas LL, Rios E, DeCoursey TE.** A pH-stabilizing role of voltage-gated proton channels in IgE-mediated activation of human basophils. *Proc Natl Acad Sci USA* 105: 11020–11025, 2008.

47. **Nakagawara A, Nathan CF, Cohn ZA.** Hydrogen peroxide metabolism in human monocytes during differentiation in vitro. *J Clin Invest* 68: 1243–1252, 1981.

48. **Nanda A, Romanek R, Curnutte JT, Grinstein S.** Assessment of the contribution of the cytochrome *b* moiety of the NADPH oxidase to the transmembrane H$^+$ conductance of leukocytes. *J Biol Chem* 269: 27280–27285, 1994.

49. **Reiss M, Roos D.** Differences in oxygen metabolism of phagocytosing monocytes and neutrophils. *J Clin Invest* 61: 480–488, 1978.

50. **Sbarra AJ, Karnovsky ML.** The biochemical basis of phagocytosis. I. Metabolic changes during the ingestion of particles by polymorphonuclear leukocytes. *J Biol Chem* 234: 1355–1362, 1959.

51. **Schilling T, Eder C.** Ion channel expression in resting and activated microglia of hippocampal slices from juvenile mice. *Brain Res* 1186: 21–28, 2007.

52. **Schrenzel J, Lew DP, Krause KH.** Proton currents in human eosinophils. *Am J Physiol Cell Physiol* 271: C1861–C1871, 1996.

53. **Schrenzel J, Serrander L, Bánfi B, Nüsse O, Fouyouzi R, Lew DP, Demaurex N, Krause KH.** Electron currents generated by the human phagocyte NADPH oxidase. *Nature* 392: 734–737, 1998.

54. **Simpson IA, Dwyer D, Malide D, Moley KH, Travis A, Vannucci SJ.** The facilitative glucose transporter GLUT3: 20 years of distinction. *Am J Physiol Endocrinol Metab* 295: E242–E253, 2008.

55. **Suzuki H, Kakinuma K.** Evidence that NADPH is the actual substrate of the oxidase responsible for the "respiratory burst" of phagocytosing polymorphonuclear leukocytes. *J Biochem* 93: 709–715, 1983.

56. **Tarasov A, Dusonchet J, Ashcroft F.** Metabolic regulation of the pancreatic β-cell ATP-sensitive K^+ channel: a pas de deux. *Diabetes* 53, *Suppl* 3: S113–S122, 2004.

57. **Tarsi-Tsuk D, Levy R.** Stimulation of the respiratory burst in peripheral blood monocytes by lipoteichoic acid. The involvement of calcium ions and phospholipase A_2. *J Immunol* 144: 2665–2670, 1990.

58. **Turpin J, Hersh EM, Lopez-Berestein G.** Characterization of small and large human peripheral blood monocytes: effects of in vitro maturation on hydrogen peroxide release and on the response to macrophage activators. *J Immunol* 136: 4194–4198, 1986.

59. **Wagner R.** Studies on the physiology of the white blood cell; the glycogen content of leukocytes in leukemia and polycythemia. *Blood* 2: 235–243, 1947.

60. **Yagisawa M, Yuo A, Yonemaru M, Imajoh-Ohmi S, Kanegasaki S, Yazaki Y, Takaku F.** Superoxide release and NADPH oxidase components in mature human phagocytes: correlation between functional capacity and amount of functional proteins. *Biochem Biophys Res Commun* 228: 510–516, 1996.